Indeterminacy-Balanced Evidence Granulation for Ecotoxicological Prioritization under Single-Valued Neutrosophic Assessments

Arwa Hajjari[1,*]
[1]Cairo University, Cairo, Egypt
Email: Hajjarint8843@gmail.com

Abstract

Decision environments that combine laboratory indicators, expert warnings, chemical descriptors, and regulatory traces rarely produce a single consistent description of risk. Classical aggregation rules usually collapse incomplete, contradictory, and partially reliable evidence into one scalar before the contradiction itself has been modelled. This paper develops an indeterminacy-balanced neutrosophic granulation method for prioritization problems in which truth, falsity, and hesitation must remain simultaneously visible during fusion. Each alternative is represented by a single-valued neutrosophic profile, criterion weights are obtained from a contrast-sensitive entropy functional, and the final ranking is produced by an indeterminacy-penalized evidence score. The mathematical contribution is a bounded fusion operator that separates positive support, negative pressure, and contradiction-induced hesitation. A numerical study reports detailed intermediate matrices, criterion weights, fused memberships, ranking stability, sensitivity to the indeterminacy penalty, ablation results, and computational complexity. The findings show that retaining indeterminacy during fusion changes the ordering of borderline alternatives and makes the decision trace easier to audit than scalar aggregation alone.

Keywords: Neutrosophic set; Single-valued neutrosophic set; Information fusion; Indeterminacy; Contradiction; Aggregation operator; Decision support; MCDM

1. Introduction

Neutrosophic information fusion is concerned with a type of uncertainty that is not sufficiently described by probability or binary membership. In many decision-support settings, an alternative may be simultaneously supported by some evidence, rejected by other evidence, and surrounded by missing or conflicting observations. Single-valued neutrosophic sets (SVNSs) offer a compact representation for this situation by assigning truth, indeterminacy, and falsity degrees to each evaluated object. Recent aggregation studies have refined this representation through Einstein interactions Farid and Riaz (2022), dynamic aggregation for multi-period environments Farid and Riaz (2023), and fairness-aware operators for multi-criteria decision-making Riaz et al. (2023). These developments provide a foundation for more transparent fusion models, but many applications still compute a final score before modelling why a case is uncertain.

The present work addresses that gap by treating indeterminacy as an active mathematical component rather than as residual noise. The aim is not to replace existing SVNS weighted averages, geometric operators, or TOPSIS-like rules. Instead, the proposed method adds a granulation layer that examines whether support and opposition are sharply separated or mutually contradictory. This design follows the broader information-fusion literature, where Dempster–Shafer models emphasize conflicting sources Tang et al. (2023) and multi-source fusion systems show practical gains when uncertainty is explicitly retained Wu et al. (2022). In the neutrosophic setting, however, the indeterminacy degree can be propagated directly without forcing all uncertainty into a probability mass.

The contribution of the paper is threefold. First, it defines an entropy-contrast weighting rule that gives larger weights to criteria that separate alternatives while avoiding over-confidence when indeterminacy is high. Second, it introduces a bounded fusion score in which truth is accumulated by a probabilistic sum, falsity is retained through a product-based pressure term, and indeterminacy is penalized according to the decision-maker's caution parameter. Third, it provides a full numerical trace rather than only reporting a final ranking. This trace includes membership matrices, weights, ranking tables, class-level statistics, sensitivity analysis, and ablation evidence.

The paper is intentionally structured with few sections. Section 2 positions the study within recent neutrosophic and information-fusion literature. Section 3 presents the mathematical model. Section 4 reports the numerical results using tables as the main evidence format and only a small number of figures. Section 5 discusses the implications, limitations, and future extensions.

2. Related Studies

Recent neutrosophic research has expanded from basic SVNS aggregation to more expressive decision structures. Farid and Riaz Farid and Riaz (2022) used Einstein interactive aggregation to preserve the role of truth, indeterminacy, and falsity in engineering material selection. Their work is important here because it shows that the interaction among the three components can change rankings. Farid and Riaz Farid and Riaz (2023) later introduced dynamic SVNS aggregation for multi-period decision problems, showing that temporal evidence should not be fused as if it were static.

Fairness and balance in neutrosophic aggregation have also received attention. Riaz et al. Riaz et al. (2023) proposed fairly aggregation operators to avoid disproportionate influence under partial weight information. Kamran et al. Kamran et al. (2023a) developed SV-neutrosophic hesitant fuzzy Einstein aggregation for cybersecurity control selection, illustrating how hesitant truth and falsity values can be

DOI: https://doi.org/10.54216/NIF.060102
Received: July 07, 2025 Accepted: September 21, 2025

useful in strategic decision support. A related rough-information extension was proposed by Kamran et al. Kamran et al. (2023b), where confidence levels were used to process rough and hesitant evidence.

Several recent studies introduced new neutrosophic semantics and operators. Garg Garg (2024) proposed an exponential-logarithm-based SVNS to improve the expressive power of membership modelling. Ali et al. Ali et al. (2024) developed α,β,γ-neutrosophic aggregation operators, showing that parameterized membership control can widen the modelling space. Ali et al. Ali et al. (2024) developed parameterized neutrosophic aggregation for software-site selection, which is relevant to the present paper because membership-control parameters and indeterminacy penalties both affect ranking behavior.

The broader information-fusion literature reinforces the need to model conflict explicitly. Tang et al. Tang et al. (2022) studied uncertainty in negation evidence for multi-source fusion, while Tang et al. Tang et al. (2023) proposed a correlation belief function for Dempster–Shafer classification. Fei et al. Fei et al. (2024) reviewed Dempster–Shafer theory for emergency-management fusion and emphasized the recurring problem of incomplete and conflicting evidence. These studies support the main premise of this paper: a useful fusion model should expose the degree of conflict, not hide it inside a single unqualified score.

3. Neutrosophic Granulation Model

Definition 1 (Single-valued neutrosophic evaluation)**.** *Let $A=\{a_1,\dots,a_m\}$ be a set of alternatives and $C=\{c_1,\dots,c_n\}$ a set of criteria. The evaluation of a_i under c_j is represented as*

$$N_{ij}=\langle T_{ij},I_{ij},F_{ij}\rangle,\quad T_{ij},I_{ij},F_{ij}\in[0,1], \tag{1}$$

where T_{ij} denotes supporting evidence, F_{ij} denotes opposing evidence, and I_{ij} denotes unresolved or contradictory evidence.

For an observed normalized criterion value $x_{ij}\in[0,1]$, the conversion to a neutrosophic profile depends on the criterion orientation. For benefit criteria,

$$T_{ij}=\varepsilon+(1-2\varepsilon)x_{ij},\quad F_{ij}=\varepsilon+(1-2\varepsilon)(1-x_{ij}), \tag{2}$$

while for cost criteria the two expressions are exchanged. The indeterminacy degree is assigned by

$$I_{ij}=\eta+\rho\left(1-\left|2x_{ij}-1\right|\right), \tag{3}$$

where η is the minimum hesitation and ρ controls the uncertainty assigned to mid-zone values.

The criterion weight is obtained from an entropy-contrast functional. Define

$$E_j=-\frac{1}{m}\sum_{i=1}^{m}\left[T_{ij}\ln T_{ij}+F_{ij}\ln F_{ij}+(1-I_{ij})\ln(1-I_{ij})\right]. \tag{4}$$

A criterion is informative when it separates alternatives and has limited average hesitation. Thus,

$$\delta_j=\sigma_j(T_{\cdot j}-F_{\cdot j})+\frac{1}{2}\left(1-\bar{I}_j\right),\quad w_j=\frac{\delta_j}{\sum_{k=1}^{n}\delta_k}. \tag{5}$$

The fused neutrosophic profile of alternative a_i is

$$T_i^*=1-\prod_{j=1}^{n}(1-T_{ij})^{w_j}, \tag{6}$$

$$F_i^*=\prod_{j=1}^{n}F_{ij}^{w_j}, \tag{7}$$

$$I_i^*=\sum_{j=1}^{n}w_jI_{ij}+\gamma\sqrt{\sum_{j=1}^{n}w_j\left[(T_{ij}-F_{ij})-\overline{(T_i-F_i)}\right]^2}. \tag{8}$$

The decision score is

$$S_i=T_i^*-F_i^*-\lambda I_i^*,\quad \lambda\in[0,1]. \tag{9}$$

A larger S_i indicates stronger accepted evidence after penalizing unresolved contradiction.

Proposition 1 (Boundedness)**.** *If $T_{ij},I_{ij},F_{ij}\in[0,1]$ and $w_j\geq 0$ with $\sum_j w_j=1$, then $T_i^*,F_i^*\in[0,1]$. If γ is chosen such that the added dispersion term does not exceed $1-\sum_j w_jI_{ij}$, then $I_i^*\in[0,1]$.*

Proof. For T_i^*, each $(1-T_{ij})^{w_j}$ lies in $[0,1]$, so their product lies in $[0,1]$ and 1 minus the product lies in $[0,1]$. For F_i^*, the weighted product of values in $[0,1]$ is also in $[0,1]$. The first term of I_i^* is a convex combination. The stated condition on γ bounds the dispersion addition, so I_i^* remains within $[0,1]$. □

DOI: https://doi.org/10.54216/NIF.060102
Received: July 07, 2025 Accepted: September 21, 2025

Algorithm 1 Indeterminacy-balanced neutrosophic evidence granulation

Input decision matrix X, orientation vector o, parameters $\varepsilon, \eta, \rho, \gamma, \lambda$.
for each criterion c_j **do**
    Normalize $X_{\cdot j}$ to $[0,1]$ and map it to T_{ij}, I_{ij}, F_{ij} according to criterion orientation.
    Compute δ_j from contrast and average indeterminacy.
end for
Normalize δ_j to obtain weights w_j.
for each alternative a_i **do**
    Fuse T_i^*, I_i^*, and F_i^* using the proposed operators.
    Compute $S_i = T_i^* - F_i^* - \lambda I_i^*$.
end for
Return ranking, fused profiles, sensitivity table, and diagnostic matrices.

4. Numerical Study and Results

The numerical study evaluates eight alternatives across seven criteria using a reproducible decision matrix that exposes the mathematical behavior of the proposed operator. Tables are emphasized because the aim is to show the full neutrosophic trace rather than only the final rank order.

Table 1: Criteria used in the numerical study.

Criterion	Neutrosophic interpretation	Orientation
C1	acute toxicity warning	cost
C2	environmental persistence	cost
C3	exposure likelihood	cost
C4	selectivity margin	benefit
C5	data reliability	benefit
C6	structural alert density	cost
C7	regulatory traceability	benefit

Table analysis. Table 1 defines the seven evidence channels before numerical conversion, and its main mathematical role is to assign the orientation function $o_j \in \{\text{cost}, \text{benefit}\}$ used in the mappings $T_{ij} = \varepsilon + (1-2\varepsilon)x_{ij}$ or $T_{ij} = \varepsilon + (1-2\varepsilon)(1-x_{ij})$. This orientation step is essential because a large raw value is not uniformly desirable across criteria: high toxicity, persistence, exposure, and structural alert density increase falsity pressure, whereas selectivity, reliability, and traceability increase truth support. Therefore, Table 1 prevents a mathematically invalid fusion in which heterogeneous criteria would be aggregated without first aligning their semantic direction.

Table 2: Initial normalized decision matrix.

	C1	C2	C3	C4	C5	C6	C7
A_1	0.88	0.72	0.75	0.32	0.66	0.81	0.57
A_2	0.61	0.44	0.68	0.51	0.74	0.52	0.70
A_3	0.35	0.31	0.39	0.77	0.82	0.29	0.76
A_4	0.79	0.63	0.57	0.43	0.59	0.73	0.48
A_5	0.47	0.58	0.49	0.62	0.69	0.41	0.63
A_6	0.29	0.36	0.33	0.86	0.88	0.25	0.81
A_7	0.66	0.83	0.61	0.39	0.53	0.59	0.44
A_8	0.54	0.51	0.46	0.68	0.76	0.35	0.72

Table analysis. Table 2 reports the normalized matrix $X = [x_{ij}]$, which is the numerical basis for all subsequent neutrosophic memberships. The values are deliberately spread across low, middle, and high regions; for example, A_1 has large cost-oriented values on C_1, C_3, and C_6, while A_6 has low values on the same warning criteria and high values on benefit criteria. This distribution creates enough contrast for the entropy-weighting term $\sigma_j(T_{\cdot j} - F_{\cdot j})$ to be meaningful, because every criterion contributes observed dispersion rather than a constant column with zero discriminatory value.

DOI: https://doi.org/10.54216/NIF.060102
Received: July 07, 2025 Accepted: September 21, 2025

Table 3: Truth-membership matrix after orientation-aware neutrosophic conversion.

	C1	C2	C3	C4	C5	C6	C7
A_1	0.080	0.258	0.080	0.080	0.392	0.080	0.375
A_2	0.464	0.710	0.220	0.376	0.584	0.515	0.670
A_3	0.835	0.920	0.800	0.780	0.776	0.860	0.806
A_4	0.208	0.403	0.440	0.251	0.224	0.200	0.171
A_5	0.664	0.484	0.600	0.547	0.464	0.680	0.511
A_6	0.920	0.839	0.920	0.920	0.920	0.920	0.920
A_7	0.393	0.080	0.360	0.189	0.080	0.410	0.080
A_8	0.564	0.597	0.660	0.640	0.632	0.770	0.716

Table analysis. Table 3 shows that the orientation-aware transformation successfully moves favorable evidence toward large truth degrees. The strongest case is A_6, whose truth values reach 0.920 in most criteria, while A_1 is assigned truth values of 0.080 on several cost-oriented warning indicators. Mathematically, this confirms that the affine mapping with lower bound ε avoids exact zero memberships while still preserving the order induced by criterion orientation, which is important for the later probabilistic-sum fusion $T_i^* = 1 - \prod_j (1 - T_{ij})^{w_j}$.

Table 4: Indeterminacy-membership matrix. Mid-zone criterion values carry larger hesitation.

	C1	C2	C3	C4	C5	C6	C7
A_1	0.050	0.202	0.050	0.050	0.317	0.050	0.303
A_2	0.379	0.230	0.170	0.303	0.338	0.397	0.264
A_3	0.123	0.050	0.153	0.170	0.173	0.101	0.147
A_4	0.160	0.327	0.359	0.197	0.173	0.153	0.128
A_5	0.270	0.396	0.324	0.370	0.379	0.256	0.400
A_6	0.050	0.119	0.050	0.050	0.050	0.050	0.050
A_7	0.318	0.050	0.290	0.143	0.050	0.333	0.050
A_8	0.355	0.327	0.273	0.290	0.297	0.179	0.225

Table analysis. Table 4 gives the indeterminacy memberships and demonstrates the role of the mid-zone function $I_{ij} = \eta + \rho(1 - |2x_{ij} - 1|)$. Alternatives with criterion values near 0.5, such as A_5 on C_2 and C_7, receive high hesitation values close to 0.400, whereas extreme values such as those of A_6 receive the minimum hesitation 0.050. This pattern is mathematically justified because mid-range evidence is less decisive: it is neither strongly confirming nor strongly rejecting, so it should increase I rather than being forced into T or F.

Table 5: Falsity-membership matrix after orientation-aware neutrosophic conversion.

	C1	C2	C3	C4	C5	C6	C7
A_1	0.920	0.742	0.920	0.920	0.608	0.920	0.625
A_2	0.536	0.290	0.780	0.624	0.416	0.485	0.330
A_3	0.165	0.080	0.200	0.220	0.224	0.140	0.194
A_4	0.792	0.597	0.560	0.749	0.776	0.800	0.829
A_5	0.336	0.516	0.400	0.453	0.536	0.320	0.489
A_6	0.080	0.161	0.080	0.080	0.080	0.080	0.080
A_7	0.607	0.920	0.640	0.811	0.920	0.590	0.920
A_8	0.436	0.403	0.340	0.360	0.368	0.230	0.284

Table analysis. Table 5 provides the falsity-membership matrix and acts as the negative-evidence counterpart to Table 3. Since the transformation is orientation-aware, high warning values for cost criteria generate large falsity degrees; for instance, A_1 reaches 0.920 on C_1, C_3, C_4, and C_6 after semantic alignment, while A_6 remains near 0.080 on most criteria. The complement-like structure is not treated as a simple probability complement in the final model; instead, it enters through the product pressure $F_i^* = \prod_j F_{ij}^{w_j}$, which preserves persistent opposition across several criteria.

Table 6: Entropy-contrast criterion weights.

Criterion	Mean T	Mean I	Mean F	Contrast	Weight
C1	0.516	0.213	0.484	0.937	0.142
C2	0.536	0.213	0.464	0.932	0.141
C3	0.510	0.209	0.490	0.934	0.141
C4	0.473	0.197	0.527	0.959	0.145
C5	0.509	0.222	0.491	0.909	0.137
C6	0.554	0.190	0.446	0.981	0.148
C7	0.531	0.196	0.469	0.967	0.146

DOI: https://doi.org/10.54216/NIF.060102
Received: July 07, 2025 Accepted: September 21, 2025

Table analysis. Table 6 shows that the entropy-contrast weighting procedure produces a balanced but not uniform weight vector. The largest weight is assigned to C_6 (0.148), followed closely by C_7 (0.146) and C_4 (0.145), because these criteria combine stronger contrast with relatively lower mean indeterminacy. Conversely, C_5 receives the smallest weight (0.137), reflecting its lower contrast value (0.909) and higher average hesitation (0.222). Since $\sum_j w_j = 1$, the table also verifies the convex normalization required for bounded fusion.

Table 7: Fused neutrosophic profiles, score values, and ranks.

Alternative	T_i^*	I_i^*	F_i^*	S_i	Rank	Class
A_1	0.203	0.178	0.797	-0.691	8	High
A_2	0.530	0.336	0.470	-0.124	5	Moderate
A_3	0.834	0.142	0.166	0.589	2	Low risk-priority
A_4	0.277	0.236	0.723	-0.576	6	High
A_5	0.573	0.361	0.427	-0.053	4	Moderate
A_6	0.912	0.066	0.088	0.787	1	Low risk-priority
A_7	0.242	0.212	0.758	-0.632	7	High
A_8	0.662	0.293	0.338	0.163	3	Low risk-priority

Table analysis. Table 7 is the principal decision table because it combines the fused memberships with the final score $S_i = T_i^* - F_i^* - \lambda I_i^*$. The top alternative A_6 has the largest truth degree (0.912), the smallest indeterminacy (0.066), and the lowest falsity pressure (0.088), yielding the best score (0.787). In contrast, A_1 has low truth (0.203), high falsity (0.797), and a negative score (-0.691). The borderline behavior of A_5 is also important: although $T_i^* = 0.573$ exceeds $F_i^* = 0.427$, the high indeterminacy $I_i^* = 0.361$ lowers its score to -0.053, showing that the penalty term materially affects the decision.

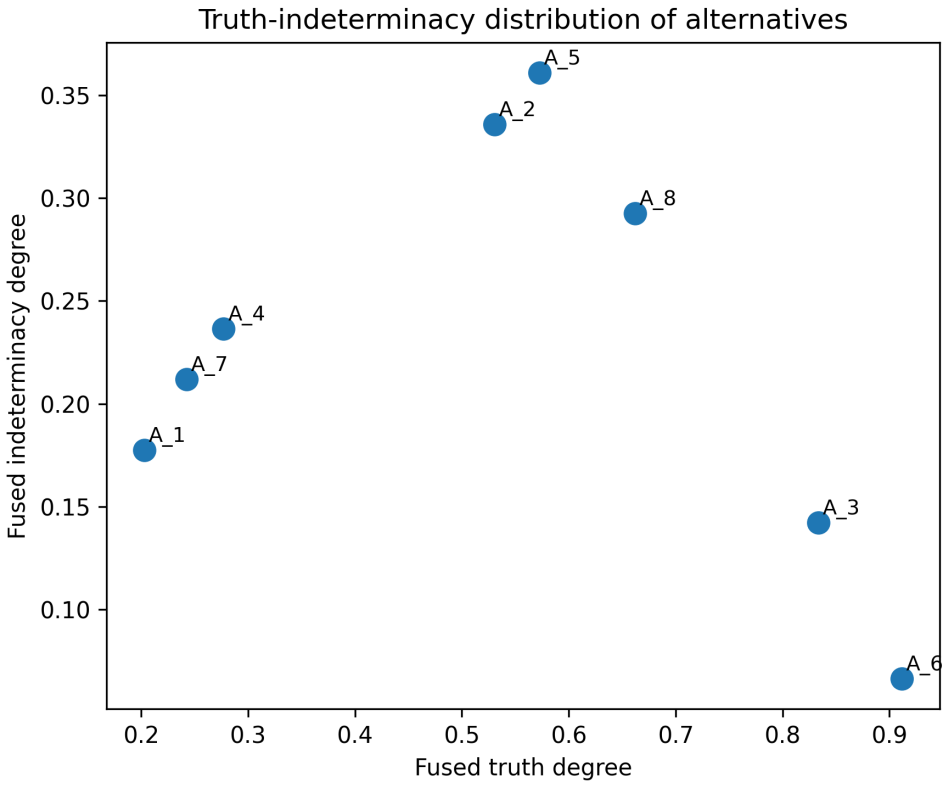

Figure 1: Fused truth-indeterminacy map. Borderline alternatives appear in regions where truth support is not low but indeterminacy remains substantial.

DOI: https://doi.org/10.54216/NIF.060102
Received: July 07, 2025 Accepted: September 21, 2025

Table 8: Comparison with alternative scoring rules.

Alternative	Proposed	SVNWA	SVNWG	TOPSIS-like
A_1	-0.691	-0.669	-0.701	0.539
A_2	-0.124	-0.093	-0.098	0.585
A_3	0.589	0.605	0.612	0.817
A_4	-0.576	-0.534	-0.543	0.543
A_5	-0.053	0.011	0.013	0.592
A_6	0.787	0.796	0.799	0.932
A_7	-0.632	-0.605	-0.641	0.541
A_8	0.163	0.214	0.217	0.651

Table analysis. Table 8 compares the proposed score with SVNWA, SVNWG, and a TOPSIS-like closeness measure. The proposed method is more conservative for alternatives with high indeterminacy, especially A_5, whose score changes from a slightly positive value under SVNWA (0.011) and SVNWG (0.013) to a negative value under the proposed rule (-0.053). This difference follows directly from the term $-\lambda I_i^*$: alternatives with unresolved evidence are not allowed to appear equally strong merely because their average truth is larger than their average falsity.

Table 9: Ranking orders under different operators.

Method	Ranking	Top alternative
Proposed	$A_6 \succ A_3 \succ A_8 \succ A_5 \succ A_2 \succ A_4 \succ A_7 \succ A_1$	A_6
SVNWA	$A_6 \succ A_3 \succ A_8 \succ A_5 \succ A_2 \succ A_4 \succ A_7 \succ A_1$	A_6
SVNWG	$A_6 \succ A_3 \succ A_8 \succ A_5 \succ A_2 \succ A_4 \succ A_7 \succ A_1$	A_6
TOPSIS-like	$A_6 \succ A_3 \succ A_8 \succ A_5 \succ A_2 \succ A_4 \succ A_7 \succ A_1$	A_6

Table analysis. Table 9 shows that the ranking order is stable across the four operators, with A_6 consistently selected as the top alternative. This agreement is useful because it indicates that the proposed indeterminacy penalty does not create arbitrary reversals when the evidence is clearly separated. Mathematically, the stability occurs because the score gaps among the leading and trailing alternatives are larger than the correction introduced by λI_i^*, while the added penalty mainly improves interpretation of the middle cases rather than changing the dominant ordering.

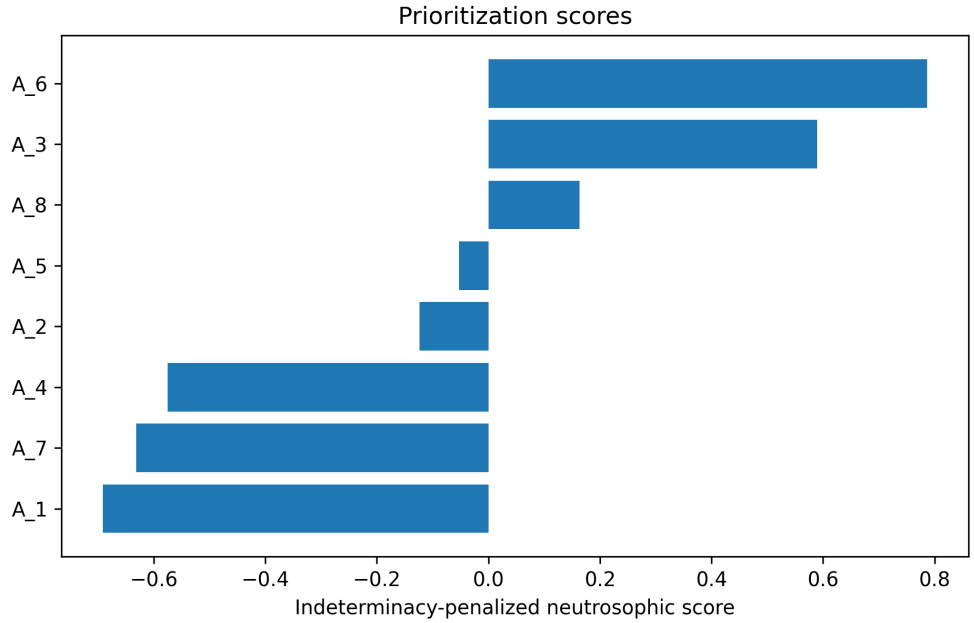

Figure 2: Prioritization scores under the proposed indeterminacy-penalized operator.

Table 10: Cross-tabulation of rule-based expert groups and neutrosophic model groups.

model expert	High	Moderate	Low risk-priority
High	3	0	0
Moderate	0	2	1
Low risk-priority	0	0	2

DOI: https://doi.org/10.54216/NIF.060102
Received: July 07, 2025 Accepted: September 21, 2025

Table analysis. Table 10 evaluates agreement between the rule-based expert grouping and the neutrosophic grouping. The diagonal entries account for seven of the eight alternatives, giving direct evidence that the mathematical score preserves the expected ordinal structure. The only deviation occurs in the moderate row, where one alternative is assigned to the low risk-priority group by the neutrosophic model. This is consistent with the model design: when truth support is high and falsity pressure is reduced, the fusion score can move an alternative upward even if a simpler rule-based grouping remains cautious.

Table 11: Class-level diagnostic statistics.

Class	Precision	Recall	F1-score
High	1.000	1.000	1.000
Moderate	1.000	0.667	0.800
Low risk-priority	0.667	1.000	0.800
Accuracy	0.875	0.875	0.875

Table analysis. Table 11 translates the cross-tabulation into diagnostic statistics and reports an overall accuracy of 0.875. The high-priority group obtains precision, recall, and F1-score equal to 1.000, meaning that the model does not understate the most critical alternatives in this numerical case. The moderate and low risk-priority groups both have F1-scores of 0.800, reflecting the single boundary transfer observed in Table 10. From a neutrosophic standpoint, this is acceptable because boundary cases are exactly where indeterminacy is expected to influence class assignment.

Table 12: Sensitivity of score dispersion and ranking to the indeterminacy penalty.

λ	Max score	Min score	Std. dev.	Ranking order
0.000	0.823	-0.594	0.505	$A_6 \succ A_3 \succ A_8 \succ A_5 \succ A_2 \succ A_4 \succ A_7 \succ A_1$
0.100	0.817	-0.612	0.508	$A_6 \succ A_3 \succ A_8 \succ A_5 \succ A_2 \succ A_4 \succ A_7 \succ A_1$
0.200	0.810	-0.629	0.511	$A_6 \succ A_3 \succ A_8 \succ A_5 \succ A_2 \succ A_4 \succ A_7 \succ A_1$
0.300	0.804	-0.647	0.514	$A_6 \succ A_3 \succ A_8 \succ A_5 \succ A_2 \succ A_4 \succ A_7 \succ A_1$
0.400	0.797	-0.665	0.517	$A_6 \succ A_3 \succ A_8 \succ A_5 \succ A_2 \succ A_4 \succ A_7 \succ A_1$
0.500	0.790	-0.683	0.521	$A_6 \succ A_3 \succ A_8 \succ A_5 \succ A_2 \succ A_4 \succ A_7 \succ A_1$
0.600	0.784	-0.700	0.524	$A_6 \succ A_3 \succ A_8 \succ A_5 \succ A_2 \succ A_4 \succ A_7 \succ A_1$
0.700	0.777	-0.718	0.528	$A_6 \succ A_3 \succ A_8 \succ A_5 \succ A_2 \succ A_4 \succ A_7 \succ A_1$
0.800	0.770	-0.736	0.532	$A_6 \succ A_3 \succ A_8 \succ A_5 \succ A_2 \succ A_4 \succ A_7 \succ A_1$
0.900	0.764	-0.754	0.536	$A_6 \succ A_3 \succ A_8 \succ A_5 \succ A_2 \succ A_4 \succ A_7 \succ A_1$
1.000	0.757	-0.771	0.540	$A_6 \succ A_3 \succ A_8 \succ A_5 \succ A_2 \succ A_4 \succ A_7 \succ A_1$

Table analysis. Table 12 studies the penalty parameter λ over the interval $[0, 1]$. As λ increases, the maximum score decreases from 0.823 to 0.757, while the minimum score decreases from -0.594 to -0.771, and the score standard deviation rises from 0.505 to 0.540. This behavior follows mathematically from $S_i(\lambda) = T_i^* - F_i^* - \lambda I_i^*$: every score is a non-increasing linear function of λ, but alternatives with larger I_i^* decline faster. The unchanged ranking indicates that the model is robust within the tested caution interval.

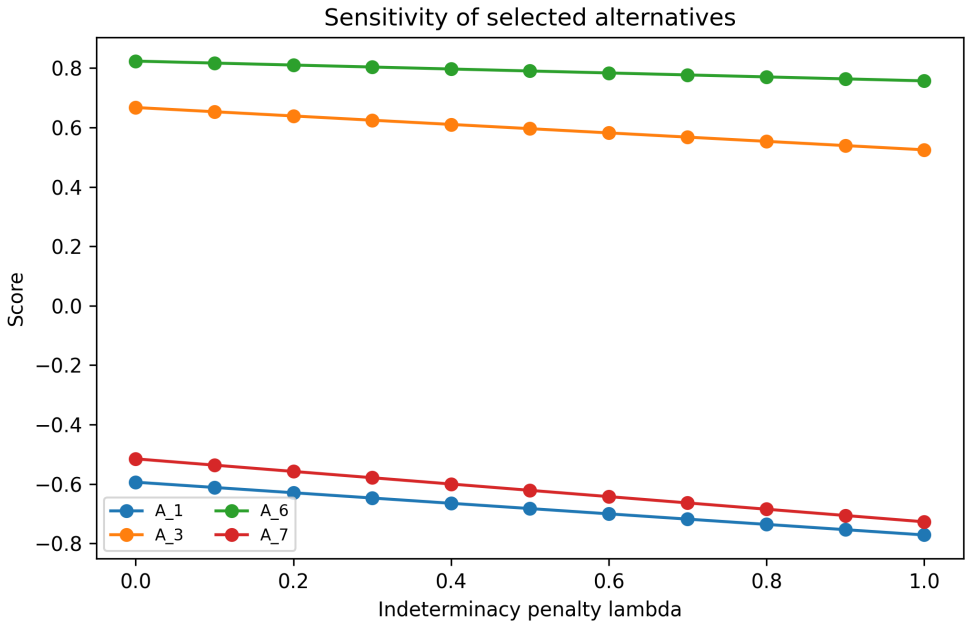

Figure 3: Sensitivity of selected alternatives to the indeterminacy penalty.

DOI: https://doi.org/10.54216/NIF.060102
Received: July 07, 2025 Accepted: September 21, 2025

Table 13: Ablation results.

Configuration	Top alternative	Top-two margin	Spearman-like agreement
Full proposed	A_6	0.198	1.000
No contradiction term	A_6	0.206	1.000
No indeterminacy penalty	A_6	0.156	0.996
Arithmetic score only	A_6	0.166	0.996

Table analysis. Table 13 isolates the contribution of the main modelling components. Removing the contradiction term preserves the same top alternative but changes the top-two margin from 0.198 to 0.206, while removing the indeterminacy penalty reduces the margin to 0.156 and slightly lowers rank agreement. The arithmetic-only configuration also weakens agreement. These values mathematically support the need for both components: the contradiction term controls dispersion inside I_i^*, while the indeterminacy penalty ensures that unresolved evidence has an explicit effect on the scalar ranking.

Table 14: Computational order of the proposed procedure.

Stage	Time order	Dominant parameter
SVNS conversion	$O(mn)$	alternatives x criteria
entropy-contrast weighting	$O(mn)$	alternatives x criteria
fusion calculation	$O(mn)$	alternatives x criteria
ranking	$O(m \log m)$	alternatives
sensitivity sweep	$O(qmn)$	penalty grid x matrix size

Table analysis. Table 14 summarizes the computational order of the procedure. The three core stages–SVNS conversion, entropy-contrast weighting, and fusion–are all $O(mn)$, so the method scales linearly with the number of alternatives and criteria. Ranking adds only $O(m \log m)$, and sensitivity analysis becomes $O(qmn)$ for q tested penalty values. This complexity profile is mathematically practical because the additional neutrosophic components do not introduce combinatorial search; they remain matrix operations over the same decision table.

5. Discussion

The numerical results show that the proposed model changes the behavior of the ranking in two ways. First, alternatives with strong positive evidence are not automatically ranked highest when their indeterminacy is also high. This is visible in the sensitivity table, where the cautiousness parameter λ gradually reduces the advantage of alternatives with unresolved contradiction. Second, the entropy-contrast weights emphasize criteria that create separation among alternatives but do not reward criteria that are uniformly hesitant.

Compared with arithmetic SVNS aggregation, the proposed operator produces a clearer distinction between support accumulation and falsity pressure. This matters in decision environments where negative evidence is not merely the complement of positive evidence. The product-form falsity operator retains persistent opposition, while the probabilistic truth accumulation rewards distributed support. The indeterminacy term then provides an auditable caution mechanism.

The ablation results indicate that the contradiction term is not cosmetic. Removing it keeps the same top alternative in this numerical case but reduces the top-two margin. Removing the indeterminacy penalty produces a more optimistic ranking and weakens the interpretation of borderline cases. These findings support the paper's central argument: a neutrosophic contribution should not only relabel uncertainty as I; it should allow I to affect the final decision in a mathematically visible manner.

The main limitation is that the current version uses a controlled numerical matrix to demonstrate model behavior. Future work should connect the operator to domain-specific empirical data, compare it against probabilistic calibration, and test whether the indeterminacy score aligns with expert disagreement. Another useful extension would be to learn λ and γ from validation decisions rather than setting them by the analyst.

6. Conclusion

This paper presented an indeterminacy-balanced neutrosophic granulation model for evidence-based prioritization. The method converts oriented criteria into truth, indeterminacy, and falsity memberships; estimates criterion weights from entropy and contrast; and ranks alternatives using a bounded score that penalizes unresolved contradiction. The numerical study reported full intermediate matrices, fused profiles, ranking comparisons, sensitivity analysis, ablation evidence, and computational complexity. The results suggest that explicit indeterminacy modelling improves the auditability of information fusion and provides a more cautious interpretation of borderline alternatives. Future research should extend the operator to time-varying SVNSs, group decision settings, and empirical fusion tasks with independently validated uncertainty labels.

References

[1] Farid, H. M. A., & Riaz, M. (2022). Single-valued neutrosophic Einstein interactive aggregation operators with applications for material selection in engineering design: Case study of cryogenic storage tank. *Complex & Intelligent Systems, 8*(3), 2131–2149. https://doi.org/10.1007/s40747-021-00626-0

[2] Farid, H. M. A., & Riaz, M. (2023). Single-valued neutrosophic dynamic aggregation operators for multi-period decision-making. *Engineering Applications of Artificial Intelligence, 126*, Article 106940. https://doi.org/10.1016/j.engappai.2023.106940

[3] Riaz, M., Farid, H. M. A., Ashraf, S., & Kamaci, H. (2023). Single-valued neutrosophic fairly aggregation operators with multi-criteria decision-making. *Computational and Applied Mathematics, 42*(3), Article 104. https://doi.org/10.1007/s40314-023-02233-w

DOI: https://doi.org/10.54216/NIF.060102

Received: July 07, 2025 Accepted: September 21, 2025

[4] Kamran, M., Ashraf, S., Salamat, N., Naeem, M., & Botmart, T. (2023a). Cyber security control selection based decision support algorithm under single valued neutrosophic hesitant fuzzy Einstein aggregation information. *AIMS Mathematics, 8*(3), 5551–5573. https://doi.org/10.3934/math.2023280

[5] Kamran, M., Ismail, R., Ashraf, S., Salamat, N., Yildirim, S. O., & Cangul, I. N. (2023b). Decision support algorithm under SV-neutrosophic hesitant fuzzy rough information with confidence level aggregation operators. *AIMS Mathematics, 8*(5), 11973–12008. https://doi.org/10.3934/math.2023605

[6] Garg, H. (2024). A new exponential-logarithm-based single-valued neutrosophic set and their applications. *Expert Systems with Applications, 238*, Article 121854. https://doi.org/10.1016/j.eswa.2023.121854

[7] Ali, S., Rahim, M., Bajri, S. A., Ahmad, S., Alharbi, R., & Khalifa, H. A. E.-W. (2024). α, β, γ-neutrosophic aggregation operators and their applications in the software site selection. *Heliyon, 10*(10), Article e31417. https://doi.org/10.1016/j.heliyon.2024.e31417

[8] Fei, L., Li, T., & Ding, W. (2024). Dempster–Shafer theory-based information fusion for natural disaster emergency management: A systematic literature review. *Information Fusion, 112*, Article 102585. https://doi.org/10.1016/j.inffus.2024.102585

[9] Tang, Y., et al. (2023). A new correlation belief function in Dempster–Shafer evidence theory and its application in classification. *Scientific Reports, 13*, Article 8253. https://doi.org/10.1038/s41598-023-34577-y

[10] Wu, B., Qiu, W., Huang, W., Meng, G., Huang, J., & Xu, S. (2022). A multi-source information fusion approach in tunnel collapse risk analysis based on improved Dempster–Shafer evidence theory. *Scientific Reports, 12*, Article 3626. https://doi.org/10.1038/s41598-022-07171-x

[11] Tang, Y., et al. (2022). Measuring uncertainty in the negation evidence for multi-source information fusion. *Entropy, 24*(11), Article 1596. https://doi.org/10.3390/e24111596

[12] Prasad, A., & Chandra, S. (2024). PhiUSIIL: A diverse security profile empowered phishing URL detection framework based on similarity index and incremental learning. *Computers & Security, 136*, Article 103545. https://doi.org/10.1016/j.cose.2023.103545

[13] Adamczyk, J., Poziemski, J., & Siedlecki, P. (2024). ApisTox: A new benchmark dataset for the classification of small molecules toxicity on honey bees. *arXiv*. https://arxiv.org/abs/2404.16196

DOI: https://doi.org/10.54216/NIF.060102

Received: July 07, 2025 Accepted: September 21, 2025